IMPROVEMENT OF THE SHAPE FUNCTION IN THE STOCHASTIC SIMULATION METHOD AND REPRODUCTION OF HIGH-FREQUENCY MOTION RECORDINGS OF THE KOBE EARTHQUAKE

Masanori Horike[1] and Yoshihiro Onishi[2]

[1] *Professor, Dept. of Architecture, Osaka Institute of Technology, Osaka, Japan*
[2] *Researcher, Geo-Research Institute, Osaka, Japan*
Email: horike@archi.oit.ac.jp,onishi@geor.or.jp

ABSTRACT:

The stochastic method is widely used to simulate high-frequency motions. However, it has a crucial defect that simulated high-frequency motions are underestimated in amplitude and duration except for near-fault zones. This is primarily caused by neglecting the contributions from multiply reflected and transmitted waves and scattered waves. We remove this defect from the method in a simple practical way. We firstly introduce an epicentral-distance dependent shaping window which is inferred from borehole data provided by KiK-net (Abbreviation of Kiban Kyoushin network). We secondly introduce the radiation coefficients transiting from theoretical to isotropic values along with propagation. The validity of this improved stochastic method is demonstrated by reproducing three-component acceleration time histories of the 1995 Hyogo-ken Nanbu earthquake (Kobe) in amplitude, duration, and spectra at all the sites in the Osaka basin.

KEY WORDS: Stochastic method, shaping window, high-frequency motions, Kobe Earthquake

1. INTRODUCTION

Wide-frequency strong ground motions are required for earthquake-hazard mitigation and earthquake-resistance design. However, numerical simulation methods based on the elasto-dynamic equations such as the finite-difference (FD) method, and the finite-element method cannot generate high-frequency motions. The hybrid method (Kamae and Irikura, 1998) is, at present, a unique practical method for computing wide-frequency strong ground motions. In general, the hybrid method sums low-frequency motions computed mostly by the FD method (For example, Graves, 1996) with high-frequency motions computed by the stochastic method (Boore, 1983).

However, there are several drawbacks in the stochastic method. The first drawback is that it generates only a single horizontal component. This drawback has already removed by Onish et al. (2004). A crucial drawback still remained is that simulated motions rapidly decrease in amplitude and duration with increasing the epicentral distance. This drawback arises from neglecting multiply reflected and transmitted waves and scattered waves generated along with propagation in inhomogeneous media.These waves have strong effects on high-frequency motions not only by way of reduction of amplitude decay (compared with amplitude decay in homogeneous media), prolongation of the duration but also by way of smear of the radiation coefficients. Therefore, the smear of the radiation coefficients is also required to introduce into the method.

The aim of this paper is to improve the stochastic method incorporating the effects of multiply reflected and transmitted waves and scattered waves and the smear of the radiation coefficients. The validity of this new method is demonstrated by reproducing accelerations of the Kobe earthquake at 8 sites in the Osaka Basin.

2. IMPROVEMENT OF THE SHAPING WINDOW AND THE RADIATION COEFFICENTS

2. 1 Inference of the parameters for the shaping window

It is difficult to numerically simulate high-frequency motions, because it requires a precise minute crustal model. Thus, an alternative approach is taken in this study. Instead of the fixed shaping window used in the conventional method, we derive an epicentral-distance dependent shaping window from the borehole recordings provided by the KiK-net network.

The shaping window used in the stochastic method is expressed as

$$s(t) = \lambda t^{\gamma/2} e^{-\alpha t/2}, \qquad (1)$$

where parameters γ and α respectively control the shape of the initial and the later portions of S waves, and $\lambda = (\alpha^{\gamma+1}/\Gamma(\gamma+1))^{0.5}$. We inferred two parameters γ and α from acceleration recordings acquired at the borehole sites of the KiK-net network. At these sites three-component accelerometers were installed on ground surface and in the borehole at a depth deeper than 100m. We selected the borehole sites, where the S wave velocity is above 1.7km/s, to reduce the contamination of surface waves as much as possible. The earthquake events and the KiK-net sites used in this study are shown in Figure 1. The Osaka Basin is surrounded with these events and sites. The focal depths of these events are between 8km and 70km and the moment magnitudes are between 3.7 and 5.6. The method for inferring the two parameters is the same as the method in Saragoni and Hart (1974). The estimates of parameter γ are not dependent on the epicental distance and the magnitude, but scatter in the range between 0.1 and 2.5. The estimates of parameter α decrease with increasing the epicentral distance, suggesting that the duration increases with increasing the epicentral distance.

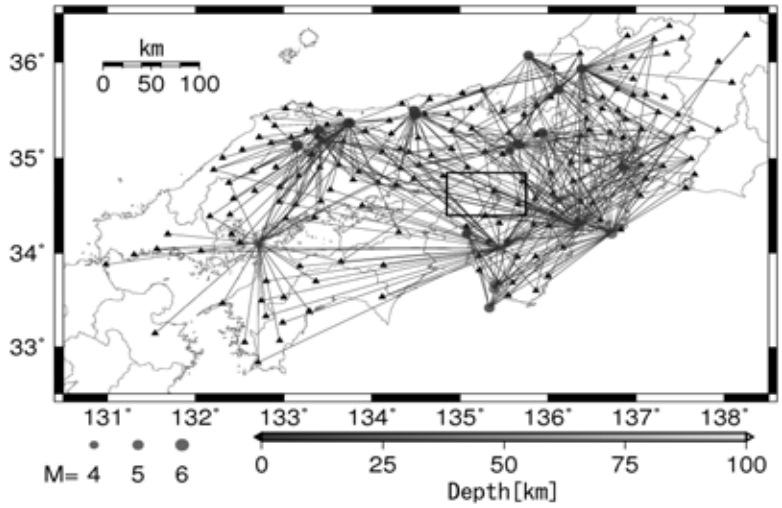

Figure 1: Earthquakes (Circles) and Kik-net sites (Triangles) used for the inference of the parameters for the shaping window. These events occurred in southwest Japan including the Osaka Basin (Rectangle).

We have already obtained the estimates for the two parameters γ and α. However, we derive the regression formula not for the two parameters γ and α but for new parameters ε and T_w, because the new parameters are obvious in physical meanings; specifically, T_w denotes the duration of the shaping window, and parameter ε denotes the ratio of time for the peak of the shaping window to the duration (Figure 2).

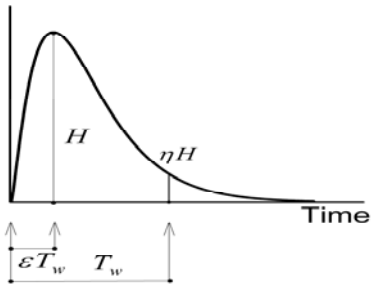

Figure 2 Schematic diagram of the shaping window for interpretation of parameters $\eta, \varepsilon,$ and T_w.

To do this, we convert parameters γ and α into parameters ε and T_w using the relations (Boore, 1983)

$$\gamma/2 = -\varepsilon \ln(\eta)/\{1+\varepsilon(\ln(\varepsilon)-1)\} \quad (2)$$

$$\alpha/2 = (\gamma/2)/(\varepsilon T_w) \quad (3)$$

We employ the same value of 0.05 for parameter η as that in Boore (1983).
Equation 2 means that parameter ε is also a fixed value because parameter γ is a fixed value. However, parameter ε is not determined as a specific value, but is confined in the range between 0.01 and 0.35 which corresponds to the range for parameter γ between 0.1 and 2.5. We derive the regression formula for parameter T_w. For this purpose the estimates of parameter α are converted into duration T_w, using equation (3). For the case of $\varepsilon = 0.2$, correspondingly $\gamma = 2.5$, converted durations T_w are shown in Figure 3. As noted, durations T_w almost linearly increase with the epicentral distance, though they scatter widely. This holds true for the other earthquakes.

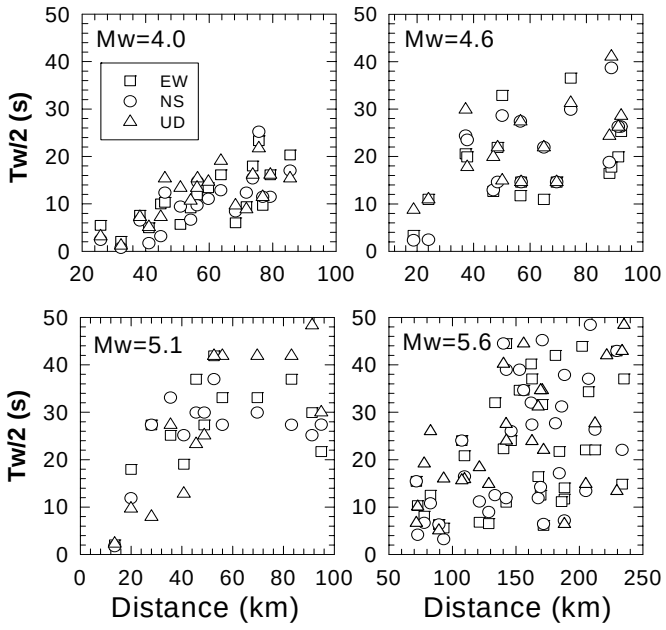

Figure 3 Parameter T_w converted from parameter α on an assumption of $\eta = 0.05$ and $\varepsilon = 0.2$.

Assuming that duration T_w is a linear function for the epicentral distance r, it is specified as

$$T_w/2 = c + Kr\,. \quad (4)$$

We estimated proportional constants K for all the earthquake by the least square fitting. Because the estimates of K appear to decrease linearly with the magnitude and, less likely, the focal depth, we derive the regression formula of K from their estimates as a linear function of the focal depth Z in unit of km and the moment magnitude M_w. The following formula is obtained,

$$K = (0.714 - 1.2\times10^{-3} Z - 6.63\times10^{-2} M_w)\,. \quad (5)$$

Since duration T_w is a sum of duration of radiated pulse $2/f_c$, where f_c is the corner frequency, and an increment along with propagation, it is expressed as,

$$T_w = 2/f_c + fct\ K\ (r - r_{off}) \tag{6}$$

where term fct, a factor dependent on parameter ε, is specified as $0.959/(1+\varepsilon(\ln(\varepsilon)-1))$. Considering that the conventional method can reproduce earthquake motions in close-fault zones (Onishi et al., 2004), we introduce r_{off} and set it at 10 km in this study.
Putting a specific value of parameters ε in the range between 0.01 and 0.35 and duration T_w calculated from the regression formula (6) into equations (2) and (3), parameters γ and α are determined. We obtain the epicental-distance-dependent shaping window by putting these new parameters into equation (1). This new shaping window can prolong the duration but still underestimate amplitude. Thus, we introduce another term into equation (1) in compensation for amplitude underestimation. The shaping window is expressed in a form of

$$s(t) = \left(\frac{T_w}{2/f_c}\right)^{\frac{n}{2}} \lambda t^{\frac{\gamma}{2}} \exp(-\frac{\alpha}{2}t), \tag{7}$$

where n does not exceed unity because a peak amplitude of the new shaping window, which is shaved off due to scattering, is less than that of the conventional (or the fixed) shaping window. Numerical experiments suggest that n is appropriate in the range between 0.5 and 0.6.

2.3 Radiation coefficients

The inhomogeneity of the propagating media affects the radiation coefficients as well. Along with propagation, the radiation coefficients, F^{SH}, F^{SV}, and F^{P} change from theoretical values dependent on the take-off angle to isotropic values expressed in equations (8) and (9) as

$$(F^{P})^2 = 4/15 \tag{8}$$

$$(F^{SV})^2 + (F^{SH})^2 = 2/5. \tag{9}$$

The manner of the transition is controlled by the statistical properties of the inhomogeneity. However, at present, we lack sufficient knowledge of these properties. Thus, we assume that the radiation coefficients change as follows

$$\begin{cases} if & D_t < L_1 W_l & theoretical\ value \\ if & L_1 W_l < D_t < L_2 W_l & Interpolation\ between\ theoretical \\ & & \quad and\ isotropic\ values \\ if & D_t > L_2 W_l & isotropic\ value \end{cases}, \tag{10}$$

where D_t and W_l denote the travel distance and the wavelength. In the computations, we assume that the factors L1 and L2 are set at 1 and 5 for P and S waves. The isotropic radiation coefficients for SH and SV waves are not the individual isotropic values, but share the same isotropic value of $1/\sqrt{5}$ derived from equation (9).
We incorporate the path effects such as geometric spreading and damping due to absorption into the method. Specifically, the geometrical spreading factors, $\Re_p$ and $\Re_s$, for P and S waves are evaluated by the dynamic ray theory (Červený et al. 1977) and the damping is evaluated along the ray paths using frequency- and depth-

dependent Q values.

2.4 Computation procedure

The moment rate function for the new stochastic method is derived by convolving the correction function (Onish et. al., 2004) with the new shaping window specified by equation (7) Using this moment rate function, we obtain acceleration time histories for the three types of body waves propagating from each sub-fault to the top of the crust. Their Fourier spectra for SH waves are expressed as

$$A_{SH}(r,f)=\left(\frac{\tilde{M}_c^{\,l}(f,r)\exp(i2\pi f t_s)}{4\pi\rho_0\beta_0^{\,3}}\right)\frac{(\rho_0\beta_0)^{0.5}}{(\rho_1\beta_1)^{0.5}}\frac{F^{SH}}{\Re_S}\exp\left(\int_{r_s}\frac{-\pi f}{\beta Q_s}dz\right), \qquad (13)$$

where $\tilde{M}_c^{\,l}(f,r)$ is the Fourier transform of the moment rate function of a subfault of a large earthquake event $d^3M_c^l(t,r)/dt^3$. Parameters ρ_0, α_0, and β_0 are the density, the P-wave velocity, and the S-wave velocity in the source region, and ρ_1, α_1, and β_1 are the density, the P-wave velocity, and the S-wave velocity at the uppermost part of the crust. Q_p and Q_s denote quality factors for P and S waves along the seismic ray paths r_p and r_s. Similar expression for SV and P waves are obtained by replacing several arguments with suitable ones. The effects of the sediments are introduced into the method as the same way described in Onishi et al. (2004).

3. SIMULATION OF KOBE EARTHQUAKE

In this section we examine the validation of the method by comparing simulated motions with strong motion recordings of the 1995 Hyogo-ken Nanbu (Kobe) earthquake at all the sites in the Osaka basin deployed by the Committee of Earthquake Observation and Research in the Kansai Area (Abbreviated as CEORKA).

3.1 Sites and Source Model

We compute accelerations at 8 sites in the Osaka sedimentary basin (Figure 3) with the new stochastic method. As described in the previous section, a one-dimensional (1-D) subsurface structure model is required at each site. Fortunately, a three-dimensional (3-D) subsurface structure model of the basin was proposed by Yamada and Horike (2007). We pick out 1-D models for the 8 sites from this 3-D model. We adopt the earthquake source model in Yamada et al. (2000). This source model has 4 asperities and their geometries are shown in Figure 4. The rupture was initiated from the bottom of the boundary between asperities 1 and 3, being denoted by the star symbol in the Figure, and after 8s the rupture of asperity 4 was initiated from the left lower corner.

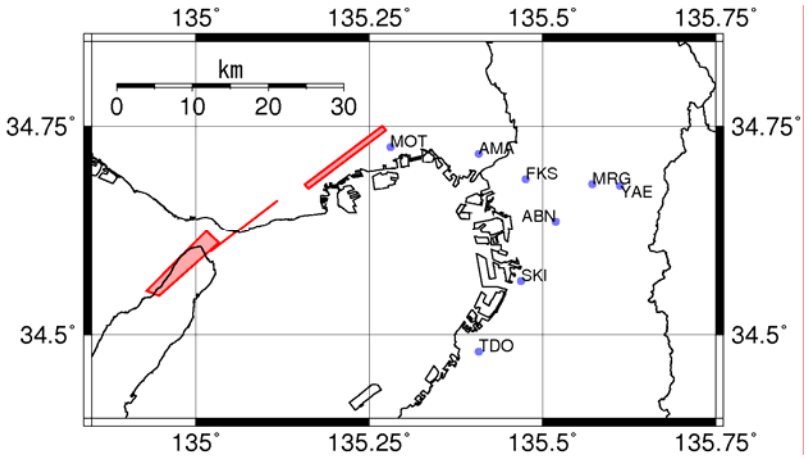

Figure 3: Map of the fault surface projection of the Kobe Earthquake (shaded area), and the 8 sites (circles).

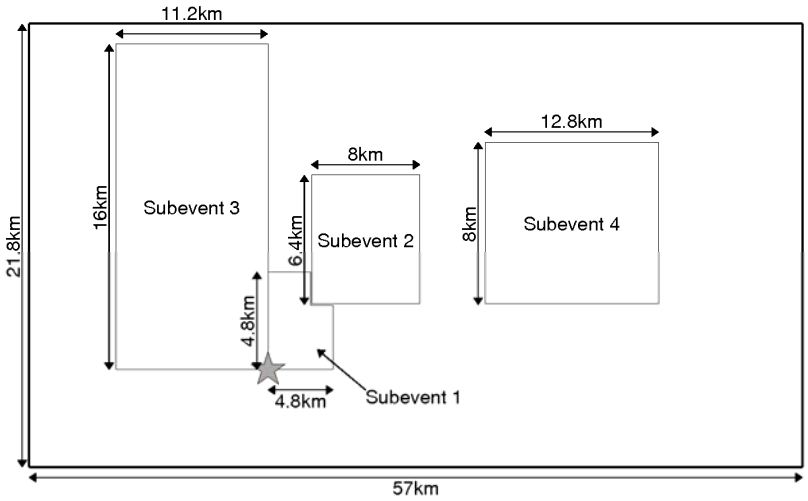

Figure 4: Source model. The four rectangles are the asperities. The star is initiation point of the fracture.

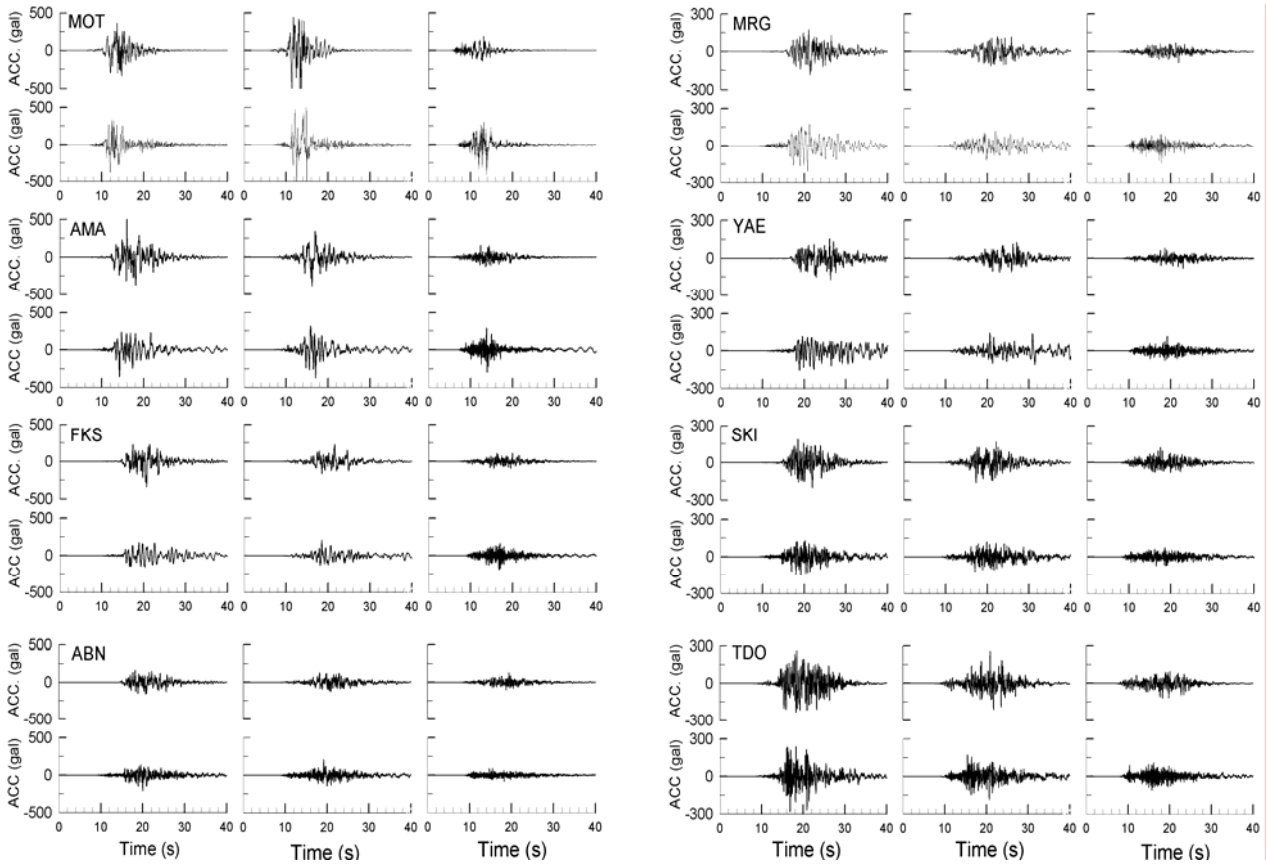

Figure 5: Comparison of the simulated (upper three traces) acceleration traces with the recorded (lower three traces) acceleration traces at the 8 sites in the Osaka Basin.

3.2 Comparison

Figure 5 shows the comparison of acceleration time histories simulated by the improved stochastic method for $\varepsilon = 0.15$ with strong motion recordings at 8 sites (See Figure 3). Simulated motions are generally similar to recorded motions in amplitude and duration for the three components at each site. Reflecting the agreement in the time histories, the acceleration spectra are also similar to each other at every site. This indicates that the improved method is a practical useful tool for simulation of high-frequency earthquake motions.

4. DISCUSSION

We showed that the improved method fairly well reproduced three-component acceleration recordings of the Kobe Earthquake at all the sites in the Osaka Basin. However, a closer look of Figure 5 reveals that the simulated vertical motions at close–fault site Mot are significantly small in amplitude, compared with recorded motions. The spectral analyses show that the cause for this is the deficiency of the vertical spectra below 0.8 Hz. Thus, we discuss the deficiency of the vertical low-frequency spectra in the followings.

We at first began with adding an extra asperity at various locations on the fault surface. However, these trials did not yield any improvement in the vertical spectra at site Mot, suggesting that fault models are not responsible for the deficiency of low-frequency vertical spectra. Besides, the radiated spectra may not be a cause either, because the two horizontal motions are reproduced well at all the sites including site Mot. As a result, we suppose that a convincing cause is the neglect of the near-field and the intermediate-field terms of the elastic wave Green's function. We show that this cause can accounts for the deficiency of the low-frequency vertical spectra at sites close to a fault such as site Mot

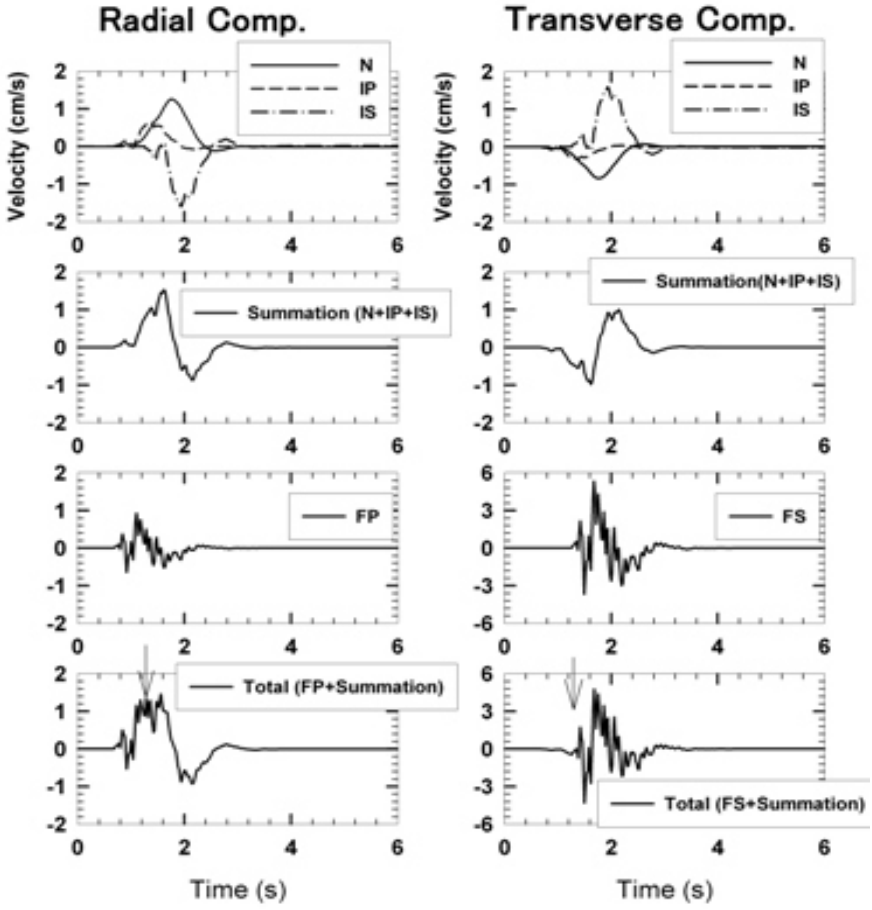

Figure 6: Comparison of the contributions from the terms of the elastic wave Green's function radiated from a point source. The four left panels are for the radial component and the four right panels are for the transverse component. The abbreviations are as follows; N: Near-field term motion, IP: Intermediate-field term P motion, IS: intermediate-field term S motion, FP: Far-field term P motion, FS: Far-field term S motion, and Total: Sum of near-field, intermediate-field, and Far-field term motions.

Using equations (4.32) in Aki and Richards (1980), we computed the velocity waveform for the individual term of the elastic wave Green's function at an epicentral distance of 5km in the homogeneous media (Figure 6). The

radiation coefficients are neglected from these waveforms because equation (4.33) in Aki and Richards (1980) ensures that the radiation coefficients are common to the terms. The source parameters for the point source were as follows; the seismic moment of $5\times10^{16}\,Nm$, the stress drop of $8MPa$, and the high frequency limit of $10Hz$. The radial motions due to the far field P (FP) term in the left third panel are appreciably small compared with the total radial motions in the left bottom panel due to the four terms of the near-field (N) term, the intermediate-field P (IP) term, the intermediate-field S (IS) term, and the far-field P (FP) term. The total radial motions are rather similar to the summation motions in the second panel due to the N term, the IP term, the IS term This accounts for the small vertical amplitude of the simulated time history at site Mot, noting that the vertical motions in close-fault zones are almost the same as the radial motions. More specifically, since the contributions from the N, IP and IS terms are not taken into account in the stochastic method, it underestimates vertical motions in close-fault zones The spectra of the far-field term are appreciably small below 0.8Hz, compared with the spectra of the total motions.

In contrast, the transverse motions due to the far-field S (FS) alone in the right third panel are quite similar in amplitude and waveform to the total transverse motions in the right second panel due to the NS, IP, IS, and FS terms, because the contribution from the N, IP, and IS term are significantly small, compared to the contribution from the FS term (See and compare the right second and the right third panels). Noting that horizontal motions in close-fault zones is almost the same as the transverse motions, the above results account for the fact that the stochastic method reproduces the horizontal motions at close-fault site Mot fairly well, despite the underestimation of the vertical motions.

5. CONCLUSION

We incorporated the effects of inhomogeneity of the propagating media such as the reduction of the amplitude decay, the prolongation of the duration, and the smear of the radiation coefficients into the method. This new method successfully reproduced the acceleration time histories and the spectra for the three components of the Kobe Earthquake at all the sites deployed by CEORKA in the Osaka basin. We think that this new stochastic method becomes a practical useful tool to generate high-frequency earthquake motions not only in close-fault areas but also wide areas encompassing earthquake faults.

REFERENCES

Aki, K., and P. G. Richards (1980). Quantitative Seismology: Theory and Method, Vol. 1, W. H. Freeman, San Francisco.

Boore, D. M. (1983). Stochastic simulation of high-frequency ground motions based on seismological models of the radiated spectra, Bull. Seism. Soc. Am., 173, 1865-1894.

Červený, V., I. A. Molotokov, and I. Pšenčík (1977). Ray method in seismology, Univerzita Karlova Praha.

Graves, R.W. (1996). Simulating seismic wave propagation in 3D elastic media using staggered-grid finite difference, Bull. Seism. Soc. Am., 86, 1091-1106.

Kamae, K. and K. Irikura (1998). Source model of the 1995 Hyogo-ken Nanbu Earthquake and simulation of near-source ground motion, Bull. Seism. Soc. Am., 88, 400-412.

Onishi, Y. M. Horike, and Y. Kawamoto.(2004). A method for simulating three-component, near-fault, strong ground motions using stochastic Green's function, DVD in 13th World Conference on Earthquake Engineering, Paper No. 2678.

Saragoni R., and G. Hart (1974). Simulation of artificial earthquakes, Earthquake Engineerings and Structural Dynamics, 2, 249-267.

Yamada, K., and Horike, M. (2007). Inference of Q-Values below 1 Hz from borehole and surface data in the Osaka basin by three-component waveform fitting, Bull. Seism. Soc. Am., 97, No.4, 1267-1278.

Yamada, M., T. Hirai, T. Iwashita, K. Kamae, K. Irikura (2000). Revision of the Hyogo-ken Nanbu earthquake source model, Abstract and Programme of 2000 Fall Meeting of the Seismological Society of Japan, A46.